Anomalous Quasiparticle Renormalization in $Na_{0.73}CoO_2$:
Role of Interorbital Interactions and Magnetic Correlations

J. Geck,[1,2] S. V. Borisenko,[1] H. Berger,[3] H. Eschrig,[1] J. Fink,[1] M. Knupfer,[1] K. Koepernik,[1] A. Koitzsch,[1]
A. A. Kordyuk,[1,4] V. B. Zabolotnyy,[1] and B. Büchner[1]

[1]*IFW Dresden, P.O. Box 270116, D-01171 Dresden, Germany*
[2]*Department of Physics and Astronomy, University of British Columbia, Vancouver, BC, V6T 1Z1, Canada*
[3]*Institut de physique de la matiére complex, EPF Lausannne, 1015 Lausanne, Switzerland*
[4]*Institute of Metal Physics of the National Academy of Sciences of Ukraine, 03142 Kyiv, Ukraine*

We report an angular resolved photoemission study of Na_xCoO_2 with $x \simeq 0.73$ where it is found that the renormalization of the quasiparticle (QP) dispersion changes dramatically upon a rotation from ΓM to ΓK. The comparison of the experimental data to the calculated band structure reveals that the quasiparticle renormalization is most pronounced along the ΓK direction, while it is significantly weaker along the ΓM direction. We discuss the observed anisotropy in terms of multiorbital effects and point out the relevance of magnetic correlations for the band structure of Na_xCoO_2 with $x \simeq 0.75$.

The unconventional behavior of correlated electrons in materials comprised of square lattices has attracted a vast amount of attention [1,2]. However, besides strong electronic correlations, the topology of the underlying lattice structure itself constitutes another important ingredient that can produce exotic electronic ground states. From this point of view, the CoO_2 layers in Na_xCoO_2 provide interesting model systems, as they constitute realizations of correlated electron systems based on a triangular lattice. More specifically, these compounds possess a layered hexagonal structure, where strongly covalent CoO_2 and ionic Na layers (*ab* planes) alternate along the perpendicular *c* axis [3]. Upon changing the Na content *x*, these materials can be doped with electrons and, in addition, water molecules can be intercalated. Both changing *x* and water intercalation drastically alter the electronic properties of Na_xCoO_2, leading most notably to the emergence of superconductivity upon hydration [4,5].

We will focus on the nonhydrated compounds with $x \simeq 0.7$, where an anomalous metallic state with an extremely large and field dependent thermoelectric power as well as a giant and field dependent electronic scattering rate was observed [6,7]. There is also evidence for the seemingly paradoxical coexistence of electron itinerancy and localized magnetic moments, as well as for unusual charge order phenomena in these macroscopically metallic compounds [8–10].

The unconventional electronic properties described above strongly motivate the study of the electronic structure of Na_xCoO_2 by means of angular resolved photoemission spectroscopy (ARPES), which provides direct and unique experimental access to single-particle excitations and, thus, to the many-body effects in these materials. Previous ARPES studies on Na_xCoO_2 [11–16] showed pronounced deviations from the electronic band structure predicted by density functional theory in the local density approximation (LDA) [17]. In addition, a strongly renormalized heavy quasiparticle (QP) band, displaying a kink feature, was reported [12–14].

In this ARPES study we focus on the momentum (k) dependent renormalization effects in $Na_{0.73}CoO_2$, which are essential to unravel the relevant couplings that govern the low energy physics. ARPES experiments were carried out using a lab-based system equipped with a SCIENTA SES 200 analyzer and a Gammadata He discharge lamp at an excitation energy $h\nu = 21.2$ eV (energy resolution 0.15 meV, angular resolution 0.2°). The high-quality $Na_{0.73}CoO_2$ single crystals examined in this study were grown by the sodium chloride flux methods as described in Ref. [18]. These samples were cleaved *in situ* at room temperature resulting in shiny cleavage surfaces. The pressure in the vacuum chamber was always kept below 5×10^{-10} mbar to prevent surface degradation. Comparing spectra taken at the beginning and the end of the experiments ensured the absence of surface aging effects during the data collection.

A typical Fermi level (E_F) crossing observed at $T = 25$ K is shown in Fig. 1, where the image on the left-hand side shows the photoelectron intensity as a function of momentum k and binding energy E_B. A single and well-defined QP band, which crosses the Fermi energy at $E_B = 0$ eV, can be observed. On the right-hand side of Fig. 1 an energy distribution curve (EDC) and a momentum distribution curve (MDC) are shown. By mapping the E_F crossings over a large area of k space, a cut through the Fermi surface (FS) of $Na_{0.73}CoO_2$ parallel to the CoO_2 planes was measured. The data allow for a precise calibration of the k scale, because dispersions from the first into the second Brillouin zone were captured. In Figs. 2(a) and 2(b) the k-dependent photoelectron intensity for two fixed binding energies of $E_B = 0$ eV and 0.132 eV are shown. Focusing on the cut at $E_B = 0$ eV in Fig. 2(a), a large hole-pocket
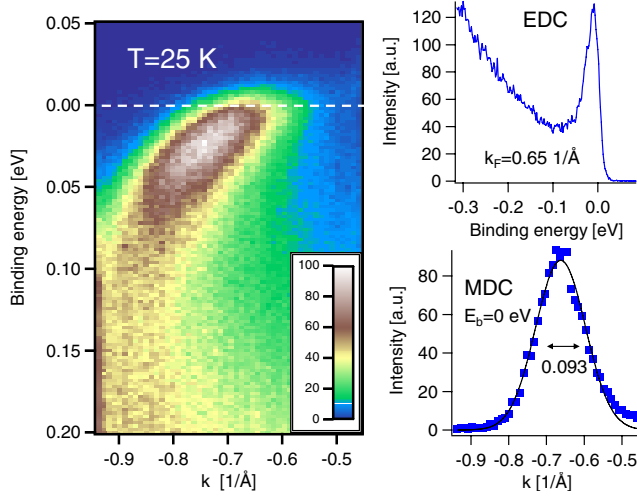
FIG. 1 (color online). Left: typical Fermi level crossing observed along a cut close to ΓM [$\psi = 173°$ cf. Fig. 2(b)] Right: corresponding energy distribution curve (EDC) and momentum distribution curve (MDC) at $k = k_F$ and $E_B = 0$ eV, respectively.

centered around the Brillouin zone center Γ is observed. The FS displays a clear hexagonal topology. Intensity variations along the FS, leading to a seemingly lower symmetry, are caused by matrix element effects. The size of the observed FS agrees well with the doping level, provided that only one of the two a_{1g} bands [cf. Fig. 2(c)] crosses E_F. This agrees with the data shown in Fig. 1, where a single QP band crosses E_F.

In accordance with previous studies, the hole pockets along ΓK are not observed for $E_B = 0$ eV. It can be seen in Fig. 2(b) that the corresponding e'_g band [cf. Fig. 2(c)] lies well below E_F, as reported earlier [14]. This can also be

observed in Fig. 2(c), where the measured band structure along ΓK and ΓM is compared to the band structure obtained by LDA [17]. While there is a fair agreement of the ARPES data and LDA at higher binding energies above 1.5 eV, deviations occur close to E_F which are particularly pronounced along ΓK.

In Fig. 3 two cuts of the data set shown in Fig. 2 along the ΓK (left) and ΓM direction (right) are shown. Focusing on the cut along ΓK, two prominent features can be observed. First, there is a band crossing E_F that forms the FS. Second, there is another band at higher binding energies, which can be identified as the e'_g band. The data indicate that the top of the e'_g band is at about 85 meV. By tracking the maximum of the MDCs for different E_B, the QP dispersion $[E(k)]$ indicated by black symbols is obtained. Close to E_F the dispersion can be well described by a linear behavior, yielding the Fermi velocity $v_F = 0.3 \pm 0.05$ eV Å along ΓK. However, at slightly higher E_B, the measured dispersion is bent and thus deviates from the linear behavior close to E_F. We define the energy where this deviation becomes significant as E_d, resulting in $E_d = (26 \pm 8)$ meV for the ΓK direction. The second bend in the dispersion around 80 meV is related to the crossing of the two bands [16]. Applying the same analysis to the cut along ΓM leads to $v_F = (0.6 \pm 0.08)$ eV Å and $E_d = (66 \pm 5)$ meV. Clearly, both v_F and E_d depend on the direction in k space.

The observed bending of the dispersion that sets in around E_d could be due to a coupling of the QP to bosonic excitations. In fact, consistent with this interpretation, we find evidence for an increased scattering rate around E_d. It has to be noted, however, that the feature in the dispersion observed here is not as well defined as the kink in the cuprates, for example. This means that the values of E_d
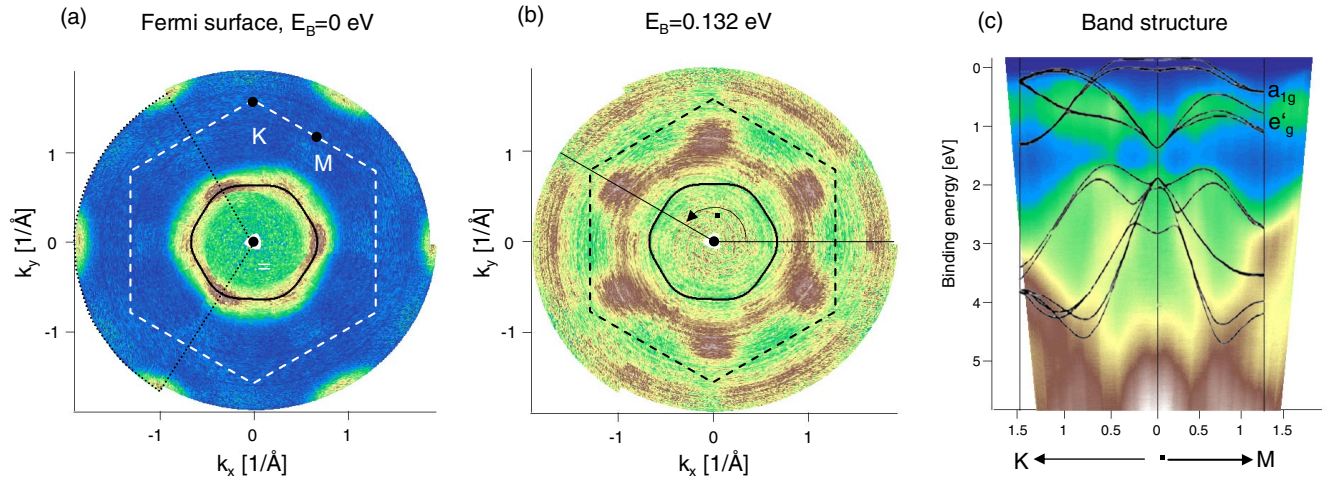

FIG. 2 (color online). ARPES data for Na₀.₇₃CoO₂ (excitation energy $h\nu = 21.2$ eV). (a), (b) Momentum distribution maps of the photoelectron intensity integrated over a small energy interval ($E_B \pm 3$ meV) at $E_B = 0$ eV and 0.132 eV measured at $T = 25$ K. The measured k region is indicated by the black dotted line in (a). The other regions in k space were obtained by rotating this data set by 120° and 240°. The broken white lines in (a) show the two-dimensional Brillouin zone. High-symmetry points Γ, K, and M are indicated in (a) and the definition of ψ is given in (b). A fit to $k_F = k_F(\psi)$ is shown as a solid black line. (c) Comparison of the measured band structure and the LDA calculation by Singh (black lines) [17]. The crystal field split e'_g and a_{1g} manifolds are indicated.
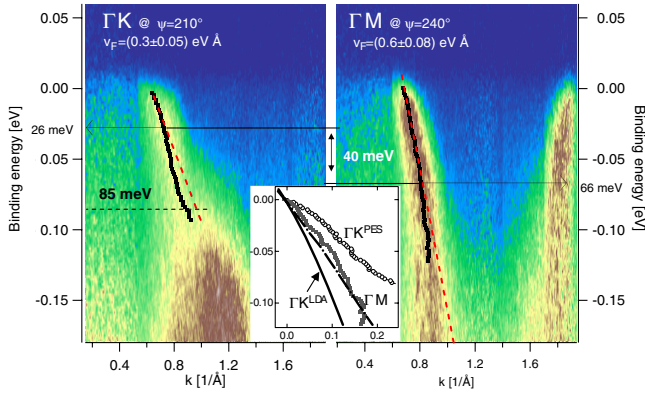
FIG. 3 (color online).   Cuts through the map data shown in
Fig. 2(a) and 2(b). The data are normalized to binding energies
above 0.25 eV. Black symbols: QP dispersion determined by
fitting MDCs at different E_B. Broken lines indicate the fitted
linear dispersions (see text). The inset shows the ARPES (sym-
bols) and LDA (lines) dispersions as a function of $k - k_F(\psi)$.
LDA for $x = 0.73$ in the rigid band approximation (cf. Fig. 4).

FIG. 4 (color online).   (a), (b) v_F^{PES} and v_F^{LDA} as a function of ψ.
The experimental v_F^{PES} values at a given value of ψ were ob-
tained by averaging over two equivalent cuts (e.g., $\psi = 150°$,
$210°$). The LDA calculations were performed in the rigid band
approximation for the low temperature lattice structure using
WIEN2K. The same behavior was also found by LDA and LSDA
calculations in the virtual crystal approximation (cf. Fig. 5).
(c) Effective mass of the QP. (a)–(c) $h\nu = 21.2$ eV. Solid curves
are fits to a sinus function intended to serve as guides to the eye.
(d) $\kappa = v_F^{\mathrm{LDA}}/v_F^{\mathrm{PES}} - 1$ characterizing the QPR.

cannot be identified straightforwardly with a specific mode
energy and, moreover, a coupling to several different bo-
sonic excitations could be possible.

In the following we will focus on v_F, which is a well-
defined quantity: cuts for different ψ values [cf. Fig. 2(b)]
were systematically analyzed in the same way as described
above. The obtained variation of v_F as determined from the
ARPES data is shown in Fig. 4(a). Upon rotating the
direction of the cut from ΓM to ΓK, v_F decreases by about
a factor of 2. Using the function $k_F(\psi)$ that was determined
from the data in Fig. 2(a) together with the obtained values
of v_F, the variation of the effective mass m^* with ψ can be
calculated. The result is given in Fig. 4(c). Remarkably, the
QP along the ΓK direction is about twice as heavy as the
QP along ΓM. This pronounced anisotropy of m^* is ex-
pected to have a strong impact on the in-plane electronic
properties of $Na_{0.73}CoO_2$.

To determine the renormalization effects in $Na_{0.73}CoO_2$,
we use the LDA band structure as a reference and compare
the ARPES Fermi velocities (v_F^{PES}) to the corresponding
LDA values (v_F^{LDA}). As it can be observed in Figs. 4(a) and
4(b), these two quantities show exactly the opposite be-
havior: v_F^{PES} decreases and v_F^{LDA} increases upon rotation
from ΓM to ΓK. In order to check whether the deviation
between ARPES and LDA is related to a lattice distortion
at the surface, LDA calculations were performed for struc-
tures where the distance between the oxygen and the cobalt
layers, i.e., the Co-O-Co bond angle, was changed. In
agreement with previous calculations, we observe that
the top of the e'_g band is shifted to higher binding energies
upon decreasing the distance between the Co and O layers
[19]. At the same time the anisotropy of v_F^{LDA} is slightly
reduced, but unchanged qualitatively. This strongly sug-
gests that the measured anisotropy of v_F^{PES} is not caused by
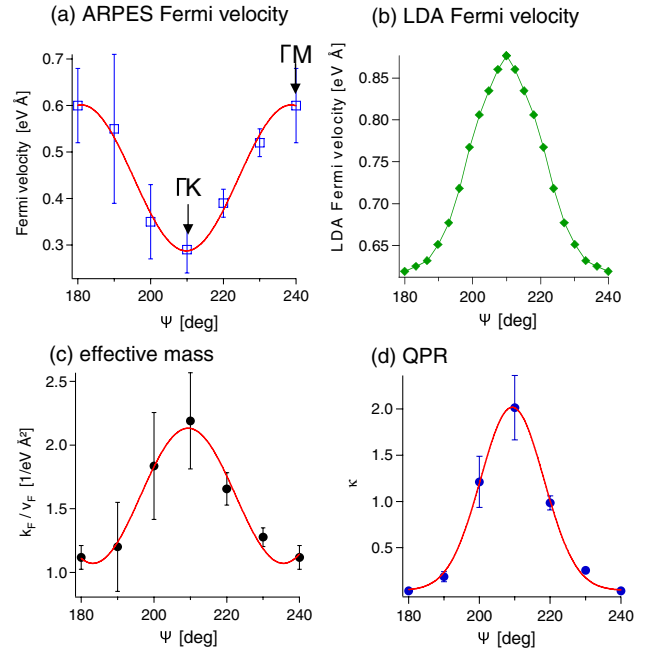a lattice distortion at the surface.

The comparison of LDA and ARPES therefore shows
that the deviation of the LDA band structure from the
measured QP dispersion increases dramatically close to
the ΓK direction (cf. inset of Fig. 3). In the following we
will refer to this deviation as QP renormalization (QPR).
This QPR can be characterized using a constant κ defined
by $(1 + \kappa)v_F^{\mathrm{PES}} = v_F^{\mathrm{LDA}}$. The ψ or, in other words, k de-
pendence, of κ is shown in Fig. 4(d), revealing the strong
anisotropy of the QPR in $Na_{0.73}CoO_2$. We note that, al-
though the photoelectron intensity in Fig. 2(a) at k_F is also
influenced by matrix element effects, it is always signifi-
cantly lower in the ΓK than in the ΓM direction, in agree-
ment with enhanced renormalization effects along ΓK.

We find $\partial_k E^{\mathrm{PES}} \simeq \partial_k E^{\mathrm{LDA}}/2$ along ΓK in the whole
energy range up to $E_B = 85$ meV (inset of Fig. 3). At the
same time it is remarkable that the QPR gets stronger the
closer the so-called e'_g band gets to the Fermi level
[cf. Fig. 2(b)]. This points to an effect related to coupling
between the a_{1g} and the e'_g bands. In fact, a strong inter-
action between these bands is manifested by a large hy-
bridization gap at higher binding energies and the
polarization dependence along ΓK found in a recent
ARPES study [16]. Hence, the k-dependent QPR at E_F is
most likely caused by multiorbital effects, i.e., interactions
between the bands labeled by e'_g and a_{1g}. In this case, the

(a) non-magnetic: 1st band   (b) non-magnetic: 2nd band

(c) antiferromagnetic   (d) AFM-FS and ARPES
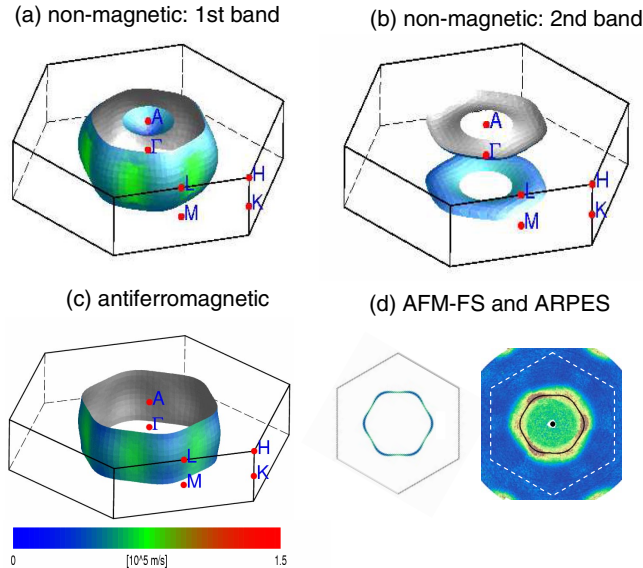
0    $[10^5 \text{m/s}]$ 1.5

FIG. 5 (color online). (a), (b) FS obtained for $x = 0.75$ by LDA in the virtual crystal approximation (VCA), revealing a three-dimensional band structure. (c) FS for the AFM ground state obtained by LSDA in the VCA where the band structure retains its pronounced two dimensionality. The color scale in (a)–(c) indicates v_F. (d) Comparison of the measured and LSDA FS. The DFT calculations have been performed using the FPLO code [23].

QP states along ΓM and ΓK display different properties: along ΓM the QP states have largely a_{1g} symmetry, while they display pronounced multiorbital properties along ΓK. This could be of crucial importance for the many-body effects in these materials, since the coupling of the QP to bosonic excitations depends critically on the symmetry of the QP states [20]. To conclude so far, the observed anisotropies clearly indicate that multiorbital effects play an important role for the QP dynamics at E_F.

Furthermore, our DFT studies—details will be provided in a forthcoming publication—show that magnetic correlations play an important role for the QP dynamics as well: according to nonmagnetic LDA calculations the band structure of $Na_{0.75}CoO_2$ displays a strong 3D character. In agreement with a previous DFT study [19], we obtain a sizeable k_z dispersion parallel to the c axis that leads to additional caps of the FS as shown in Figs. 5(a) and 5(b). Such a strong 3D character is not in agreement with ARPES data: (i) in general, the QP peaks at E_F are expected to be considerably broadened in a 3D system, in particular, because the short lifetime of the final states becomes important [21]. This is not the case (Fig. 1). (ii) ARPES measurements at various excitation energies do not show any evidence for a strong dispersion along c [16].

However, magnetic LSDA calculations yield an AFM ground state, where ferromagnetic ab planes are coupled antiferromagnetically along c. This agrees well with neutron data [22]. In the AFM state, the k_z dispersion is strongly reduced, which removes the aforementioned FS caps and yields the FS shown in Fig. 5(c). In other words, according to LSDA, 3D AFM correlations render the electronic structure of $Na_{0.75}CoO_2$ effectively 2D. The top of the e'_g band at $E_B \simeq 70$ meV as well as the topology and size of the FS obtained in LSDA are in good agreement with the ARPES data as demonstrated in 5(d). The above results together with the neutron data indicate that AFM correlations have a strong influence on the electronic structure of Na_xCoO_2 with $x \simeq 0.75$.

In conclusion, we have shown that the QPR in $Na_{0.73}CoO_2$ is strongly anisotropic and provided clear evidence for the relevance of multiorbital effects for the QP dynamics in this material. In addition, detailed DFT studies highlight the impact of magnetic correlations on the QP states near E_F, which is expected to be directly related to the unusual temperature as well as the field dependencies of the thermopower and the QP scattering rates [6,7,13]. Hence, both the interactions between the a_{1g}- and e'_g-like states as well as magnetic correlations have to be taken into account in order to obtain a realistic description of these materials.

[1] J. Orenstein and A. Millis, Science **288**, 468 (2000).
[2] Y. Tokura and N. Nagaosa, Science **288**, 462 (2000).
[3] Q. Huang *et al.*, Phys. Rev. B **70**, 184110 (2004).
[4] M. L. Foo *et al.*, Phys. Rev. Lett. **92**, 247001 (2004).
[5] K. Takada *et al.*, Nature (London) **422**, 53 (2003).
[6] Y. Wang *et al.*, Nature (London) **423**, 425 (2003).
[7] S. Li *et al.*, Phys. Rev. Lett. **93**, 056401 (2004).
[8] J. Gavilano *et al.*, Phys. Rev. B **69**, 100404(R) (2004).
[9] C. Bernhard *et al.*, Phys. Rev. Lett. **93**, 167003 (2004).
[10] F. Ning *et al.*, Phys. Rev. Lett. **93**, 237201 (2004).
[11] T. Valla *et al.*, Nature (London) **417**, 627 (2002).
[12] H.-B. Yang *et al.*, Phys. Rev. Lett. **92**, 246403 (2004).
[13] M. Z. Hasan *et al.*, Phys. Rev. Lett. **92**, 246402 (2004).
[14] H.-B. Yang *et al.*, Phys. Rev. Lett. **95**, 146401 (2005).
[15] D. Qian *et al.*, Phys. Rev. Lett. **96**, 046407 (2006).
[16] D. Qian *et al.*, Phys. Rev. Lett. **97**, 186405 (2006).
[17] D. J. Singh, Phys. Rev. B **61**, 13 397 (2000).
[18] M. Iliev *et al.*, Physica (Amsterdam) **402C**, 239 (2004).
[19] M. D. Johannes *et al.*, Europhys. Lett. **68**, 433 (2004).
[20] T. P. Devereaux *et al.*, Phys. Rev. Lett. **93**, 117004 (2004).
[21] H. Starnberg *et al.*, Phys. Rev. B **48**, 621 (1993).
[22] L. M. Helme *et al.*, Phys. Rev. Lett. **94**, 157206 (2005).
[23] K. Koepernik and H. Eschrig, Phys. Rev. B **59**, 1743 (1999).